JCS ePress online publication date 18 October 2005

Paracellin-1 and the modulation of ion selectivity of tight junctions

Jianghui Hou[1], David L. Paul[2] and Daniel A. Goodenough[1,*]

[1]Department of Cell Biology, Harvard Medical School, 240 Longwood Avenue, Boston, MA 02115, USA
[2]Department of Neurobiology, Harvard Medical School, 200 Longwood Avenue, Boston, MA 02115, USA
*Author for correspondence (e-mail: daniel_goodenough@hms.harvard.edu)

Accepted 11 August 2005
Journal of Cell Science 118, 5109-5118 Published by The Company of Biologists 2005
doi:10.1242/jcs.02631

Summary

Tight junctions play a key selectivity role in the paracellular conductance of ions. Paracellin-1 is a member of the tight junction claudin protein family and mutations in the paracellin-1 gene cause a human hereditary disease, familial hypomagnesemia with hypercalciuria and nephrocalcinosis (FHHNC) with severe renal Mg^{2+} wasting. The mechanism of paracellin-1 function and its role in FHHNC are not known. Here, we report that in LLC-PK1 epithelial cells paracellin-1 modulated the ion selectivity of the tight junction by selectively and significantly increasing the permeability of Na^+ (with no effects on Cl^-) and generated a high permeability ratio of Na^+ to Cl^-. Mutagenesis studies identified a locus of amino acids in paracellin-1 critical for this function. Mg^{2+} flux across cell monolayers showed a far less-pronounced change (compared to monovalent alkali cations) following exogenous protein expression, suggesting that paracellin-1 did not form Mg^{2+}-selective paracellular channels. We hypothesize that in the thick ascending limb of the nephron, paracellin-1 dysfunction, with a concomitant loss of cation selectivity, could contribute to the dissipation of the lumen-positive potential that is the driving force for the reabsorption of Mg^{2+}.

Supplementary material available online at
http://jcs.biologists.org/cgi/content/full/118/21/5109/DC1

Key words: Paracellin-1, Ion selectivity, Tight junction, Hypomagnesemia

Introduction

The existence of separate fluid compartments with different ionic and molecular compositions is fundamental to the biology of multicellular organisms. Compartments are delineated by epithelia that permit regulated exchange between their apical and basolateral surfaces by both transcellular (through the cytoplasm) and paracellular (between the cells) routes. Tight junctions are cell-cell interactions that provide the primary barrier to the diffusion of solutes through the paracellular pathway, and create an ion-selective boundary between the apical and basolateral extracellular compartments (for reviews, see Tsukita et al., 2001; Schneeberger et al., 2004; Anderson et al., 2004).

Epithelial paracellular permeability has been studied physiologically for decades. It has been demonstrated that simple epithelia show wide variations in their passive ion permeability (Fromter and Diamond, 1972). Claude and Goodenough suggested that the variability in junctional ion permeability might be inversely correlated with the number of anastomosing intramembranous strands that form the basic structure of tight junction visible using freeze fracture techniques (Claude and Goodenough, 1973). In order to explain the exponential relationship between the numbers of strands and the passive resistance across the junction, Claude presented an analysis in which the tight junction was modeled as having pores or ion selective channels with variable open probabilities (Claude, 1978). More recently, Tang and Goodenough demonstrated that the pathway permitting paracellular flux of the principal extracellular ions showed classical channel properties, including an ~6 Å diameter, ion selectivity, anomalous mole fraction effect and pH dependence (Tang and Goodenough, 2003).

The integral membrane proteins of tight junctions include occludin (a 65 kDa membrane protein bearing four transmembrane domains and two extracellular loops) and claudins (consisting of a family of at least 22 homologous proteins of 20-28 kDa and sharing a common topology with occludin) (Furuse et al., 1993; Furuse et al., 1998a; Furuse et al., 1998b; Morita et al., 1999). Claudins have been shown to confer ion selectivity to the paracellular pathway. Studies have shown that claudin-4, -5, -8, -11 and -14 selectively decrease the permeability of cations through tight junctions (Yu et al., 2003; Colegio et al., 2002; Van Itallie et al., 2001; Ben-Yosef et al., 2003; Wen et al., 2004), whereas claudin-2 and -15 increase cation permeability (Furuse et al., 2001; Amasheh et al., 2002; Van Itallie et al., 2003). Paracellin-1, also known as claudin-16, has been identified as a renal tight junction protein that is mutated in patients with the inherited disorder FHHNC (familial hypomagnesemia with hypercalciuria and nephrocalcinosis) (Simon et al., 1999). The expression of paracellin-1 is restricted to the thick ascending limb (TAL) of the nephron where the reabsorption of Mg^{2+} occurs predominantly by paracellular flux, a process driven by a lumen-positive transepithelial potential. The conductance of this paracellular pathway is highly regulated, with renal Mg^{2+} excretion varying from 0.5 to 80% of the filtered load

Journal of Cell Science

Journal of Cell Science

responding to low or high serum Mg^{2+} concentrations, respectively (for reviews, see Greger, 1985; De Rouffignac and Quamme, 1994). It was hypothesized that paracellin-1 constitutes the core of an intercellular pore, allowing the paracellular electrophoresis of Mg^{2+} driven by the transepithelial potential (Simon et al., 1999). Numerous studies have since followed identifying more points of mutation in paracellin-1 linked to FHHNC (Weber et al., 2001a; Blanchard et al., 2001; Muller et al., 2003).

Definitive determination of the function of paracellin-1 depends on the expression of paracellin-1 in epithelial cell models well established to allow the measurement of junctional ion permeability. In this study, we have expressed paracellin-1 in a series of cell models and probed the function of paracellin-1. We have also identified the structural requirements of the function of paracellin-1 and provided some mechanistic insights. Attempts to express full-length human paracellin-1 in several epithelial cell lines resulted in both low expression and failure to locate at the plasma membrane. Human paracellin-1 truncated at M71, however, showed the expected localization and function.

Materials and Methods

Antibodies

The following antibodies were used in this study: rabbit polyclonal anti-claudin-1, anti-claudin-2, anti-claudin-3, anti-claudin-14, anti-paracellin-1 and rabbit anti-ZO-1; mouse monoclonal anti-claudin-4 and anti-occludin antibodies (Zymed Laboratories); fluorescein isothiocyanate-labeled goat anti-rabbit immunoglobulin G and Rhodamine-labeled goat anti-mouse immunoglobulin G (Chemicon); and horseradish peroxidase-labeled donkey anti-rabbit immunoglobulin G and donkey anti-mouse immunoglobulin G (Amersham Pharmacia Biotech).

Cell lines

MDCK-II cells were a kind gift from Vivian Tang (Harvard Medical School, Boston, MA). 293T cells were from Joan Brugge (Harvard Medical School). LLC-PK1 cells were obtained from ATCC. Cell culture conditions were: LLC-PK1, Dulbecco's modified Eagle's medium (DMEM, Invitrogen) supplemented with 10% fetal bovine serum (FBS, Hyclone), penicillin (100 U/ml) and streptomycin (100 μg/ml) (Invitrogen); MDCK-II, Minimum Eagle's medium (MEM, Invitrogen) supplemented with 10% FBS and penicillin/streptomycin; 293T, DMEM supplemented with 10% FBS, penicillin/streptomycin and 1 mM sodium pyruvate.

Molecular cloning and retrovirus production

The following full-length mammalian claudins were cloned into the retroviral vector pLNCX2 (a kind gift of Joan Brugge, Harvard Medical School): human paracellin-1 (GenBank accession number AF152101), mouse paracellin-1 (AF323748). The site-directed mutagenesis was performed with a PCR-based mutagenesis method (Stratagene). Molecular clones for each of the mutants were verified by DNA sequencing. VSV-G-pseudotyped retroviruses were produced by transfection of the 293T cell line with pLNCX2-based constructs and plasmids encoding three retroviral structural proteins (VSV-G, Gag and Pol; a kind gift from Joan Brugge). The retrovirus-containing supernatants were collected at day 3 following transfection and used for infection of target cells.

Protein electrophoresis and immunoblotting

Confluent cells were dissolved in lysis buffer (50 mM Tris-HCl pH 7.5, 150 mM NaCl, 1% SDS and protease inhibitor cocktail; Pierce). After shearing with a 23-gauge needle, lysates (containing 15 μg total protein) were subjected to SDS-PAGE under denaturing conditions and transferred to a nitrocellulose membrane, followed by blocking with 3% milk, incubation with primary antibodies (1:1,000) and the horseradish peroxidase-labeled secondary antibody (1:5000) and exposure to an ECL Hyperfilm (Amersham). Molecular mass was determined relative to protein markers (BioRad).

Immunolabeling and confocal microscopy

Cells grown on coverslips or Transwell inserts (Corning) were fixed with cold methanol at –20°C, followed by blocking with PBS containing 10% fetal bovine serum, incubation with primary antibodies (1:300) and fluorescein isothiocyanate (FITC) or Rhodamine-labeled secondary antibodies. After washing with PBS, slides were mounted with Mowiol (CalBiochem). Indirect immunofluorescence was performed on a Nikon TE300 microscope equipped with a Plan-Neofluar 40× (NA 1.3 oil) objective and a mercury lamp and CCD camera. Confocal analyses were performed using the Nikon TE2000 confocal microscopy system equipped with Plan-Neofluar 40× (NA 1.3 oil) and 63× (NA 1.4 oil) objectives and krypton-argon laser (488 and 543 lines). For the dual imaging of FITC and Rhodamine, fluorescent images were collected by exciting the fluorophores at 488 nm (FITC) and 543 nm (Rhodamine) with argon and HeNe lasers respectively. Emissions from FITC and Rhodamine were detected with the band-pass FITC filter set of 500-550 nm and the long-pass Rhodamine filter set of 560 nm, respectively. All images were converted to JPEG format and arranged using Photoshop 6.0 (Adobe).

Electrophysiological measurements

Electrophysiological studies were performed on cell monolayers grown on porous filters (Transwell). Voltage and current clamps were performed using the EVC4000 Precision V/I Clamp (World Precision Instruments) with Ag/AgCl electrodes and an Agarose bridge containing 3 M KCl. Transepithelial resistance (TER) was measured using the Millicell-ERS and chopstick electrodes (Millipore). All experiments were conducted at 37°C. TER of the confluent monolayer of cells was determined in buffer A (145 mM NaCl, 2 mM $CaCl_2$, 1 mM $MgCl_2$, 10 mM glucose and 10 mM HEPES, pH 7.4) and the TER of blank filters was subtracted. Dilution potentials were measured when buffer B (80 mM NaCl, 130 mM mannitol, 2 mM $CaCl_2$, 1 mM $MgCl_2$, 10 mM glucose and 10 mM HEPES, pH 7.4) replaced buffer A on the apical side or basal side of filters. Electrical potentials obtained from blank inserts were subtracted from those obtained from inserts with confluent growth of cells. The ion permeability ratio (η) for the monolayer was calculated from the dilution potential using the Goldman-Hodgkin-Katz equation:

$$\eta = -(\epsilon - e^{\nu})/(1 - \epsilon e^{\nu}) ,$$

where η is the ratio of permeability of the monolayer to Na^+ over the permeability to Cl^- ($\eta = P_{Na}/P_{Cl}$); ϵ is the dilution factor ($\epsilon = C_{basal}/C_{apical}$); $\nu = eV/kT$ (V is the dilution potential, k is the Boltzmann constant, e is the elementary charge and T is the Kelvin temperature). By Ohm's law, the total conductance, G, of the membrane can be measured. The absolute permeabilities of Na^+ (P_{Na}) and Cl^- (P_{Cl}) were calculated by using the Kimizuka-Koketsu equation,

$$P_{Na} = (G/C)\cdot(RT/F^2)\cdot\eta/(1 + \eta)$$

$$P_{Cl} = (G/C)\cdot(RT/F^2)/(1 + \eta) ,$$

where C is the concentration, R is the gas constant and F is the Faraday constant.

The permeabilities for Li^+, K^+, Rb^+ and Cs^+ were measured as for Na^+ (with the chemical gradient of 145 mM to 80 mM). The

permeability of Mg^{2+} (P_{Mg}) across monolayers was determined according to Tang and Goodenough (Tang and Goodenough, 2003).

Statistical analyses

The significance of differences between groups was tested by ANOVA (Statistica 6.0). When the all-effects F value was significant ($P<0.05$), post-hoc analysis of differences between individual groups was made with the Neuman-Keuls test. Values were expressed as mean±s.e. unless otherwise stated.

Results

Translational start site of paracellin-1

The human paracellin-1 gene encodes a 305 amino acid protein that possesses two in-frame start codons (ATG: encoding methionine M1 and M71 respectively) at the 5′-end in a suitable Kozak consensus sequence (Fig. 1A). The second ATG corresponds to the start codon of mouse and rat paracellin-1 (Fig. 1B) (Weber et al., 2001b). The similarity of the sequence downstream of amino acid M71 is high among all three species. Genetic analysis of human paracellin-1 reveals a 16.7% polymorphism at amino acid position 55 that would result in a frame shift and premature translation stop at position 90, indicating that translation of human paracellin-1 is initiated from the second ATG at M71 (Weber et al., 2001a). To confirm the translational initiation start site of human paracellin-1, we have generated a series of expression constructs in which an HA epitope tag was appended to either the N- or the C-terminus of the full-length human paracellin-1 (FL) and its truncated form (△70). In addition, we have also made constructs to express untagged human paracellin-1 (FL and △70) and mouse paracellin-1 (Fig. 1C). These constructs were transfected into both canine (MDCK-II) and human cell lines (HEK-293), and probed with an HA antibody or an antibody raised against the C-terminus of human paracellin-1. Immunoblotting of the whole cell lysate following transfection with paracellin-1 HA-tagged at the N-terminus allowed a preliminary visualization of the electrophoretic mobility of paracellin-1 (Fig. 1D, left panels). The 33 kDa band matched the predicted molecular weight of paracellin-1 (FL, amino

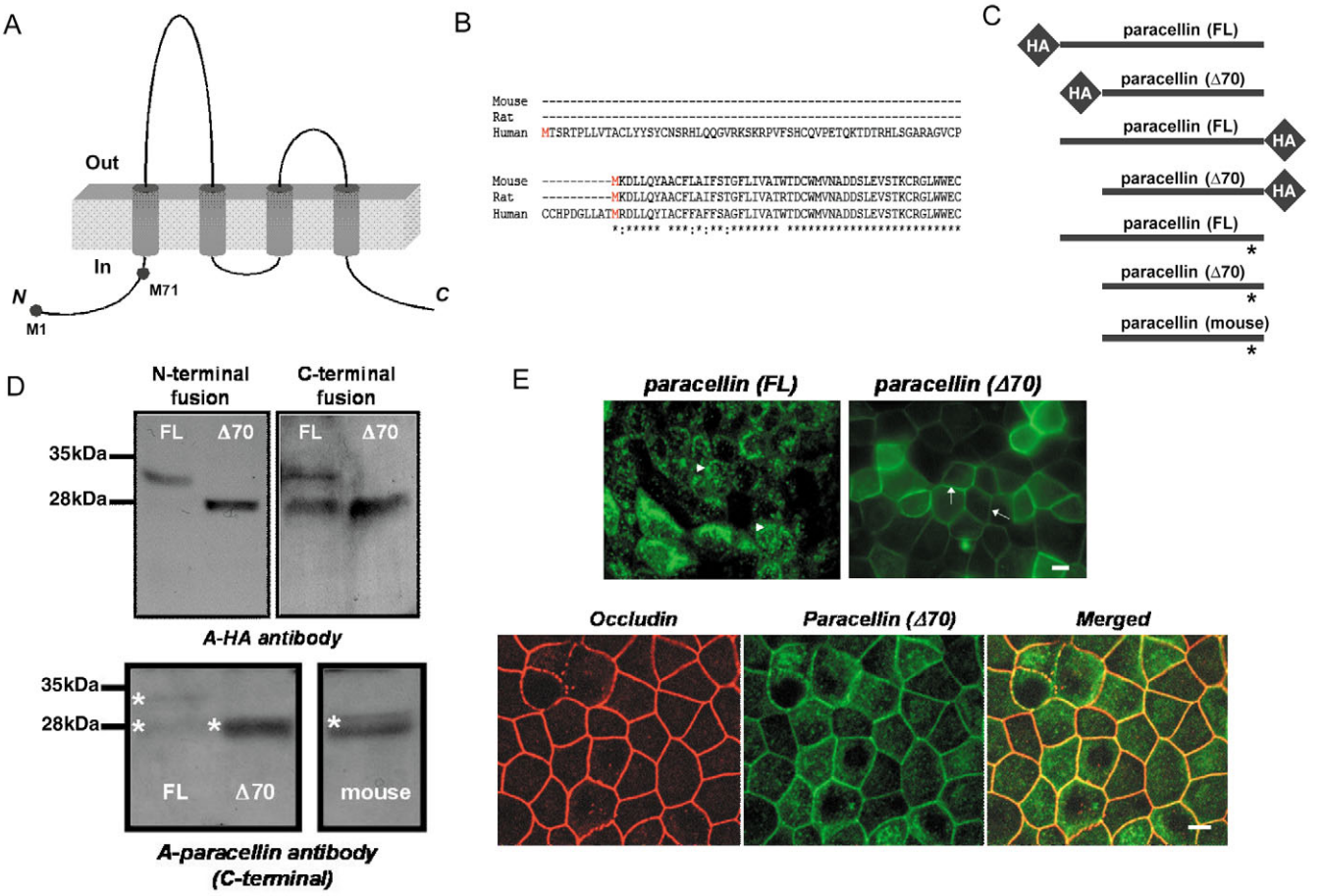

Fig. 1. Translational start site of paracellin-1. (A) The structure of paracellin-1. (B) Comparison of amino acid sequence of paracellin-1 across the species of mouse, rat and human. Note that the human sequence possesses two in-frame methionines with the second methionine highly conserved throughout the species. (C) A series of retroviral constructs for expression of the paracellin-1 gene. (D) Western immunoblots of MDCK cells infected with retrovirus expressing the constructs in C. Note that both methionines (M1 and M71) in human paracellin-1 initiate translation, suggestive of an internal ribosomal entry site (IRES) downstream of the ATG (encoding M1) in the mRNA transcripts. Positions of molecular mass markers in kDa are indicated. (E) Top panels, paracellin-1 subcellular localization. Note that the full-length paracellin-1 is mis-targeted to lysosomes (arrowheads). In contrast, paracellin-1 △70 is localized at cell-cell junctions (arrows). Bottom panels, paracellin-1 △70 colocalizes with occludin at tight junctions. Red, occludin staining; green, paracellin-1 staining; yellow to orange, colocalization of occludin and paracellin-1 in the merged panel. Bar, 10 μm.

acids 1-305) and the 27 kDa band matched △70 (amino acids 71-305). As expected, only the 33 kDa form could be detected in the N-terminally tagged transfectant. Detection of non HA-tagged protein using the antibody against the C-terminus of paracellin-1 also permitted the visualization of the alternative initiation of translation (Fig. 1D, right panels). Expression of human FL paracellin-1 (untagged or tagged with HA at the C-terminus) yielded two bands at 33 kDa and 27 kDa, corresponding to amino acids 1-305 and 71-305, respectively. In contrast, expression of human paracellin-1 △70 or mouse paracellin-1 gave rise to one band at 27 kDa. In both human and mouse cases, the lack of the first start site resulted in a more robust expression of the 27 kDa polypeptide. Our data suggest the possibility of an internal ribosomal entry site (IRES) downstream of the ATG (encoding M1) in the mRNA transcript.

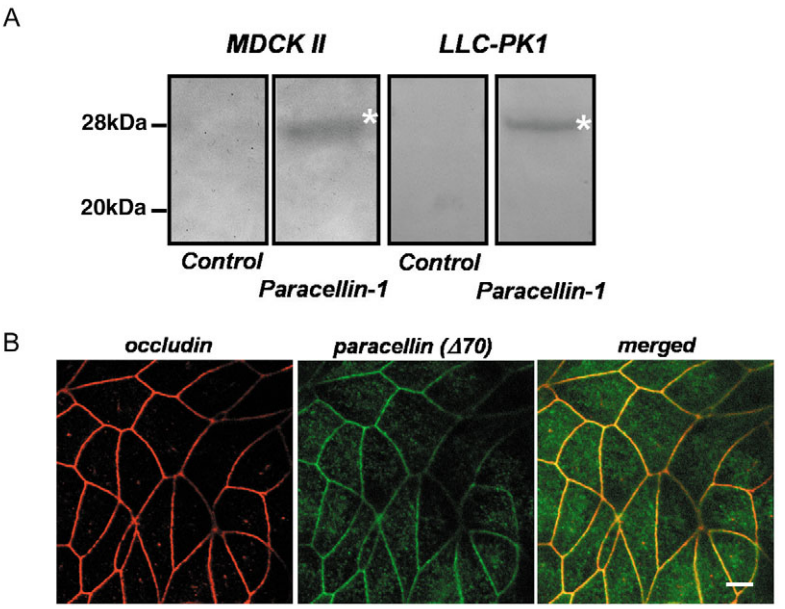

Fig. 2. Expression and localization of paracellin-1. (A) Constitutive expression of paracellin-1 in MDCK-II and LLC-PK1 cells. Paracellin-1 migrates as a 27 kDa band (*). (B) Confocal microscopy reveals the colocalization of paracellin-1 with occludin at the tight junction. Red, occludin staining; green, paracellin-1 staining; yellow to orange, colocalization of occludin and paracellin-1 on the merged panel. Bar, 10 μm.

Subcellular localization of paracellin-1

To visualize the subcellular localization of the two products of human paracellin-1 mRNA translation, we attached GFP tags to the N-terminus of the FL and △70 products and expressed each separately. Cells ectopically expressing GFP-FL- or GFP-△70-paracellin-1 were plated onto semi-permeable membranes to allow them to become fully polarized. Fluorescence images revealed that △70-paracellin-1 concentrated at cell-cell borders whereas the FL-paracellin-1 was targeted to endosomes or lysosomes (Fig. 1E, top). Confocal microscopy revealed that △70-paracellin-1 colocalized with occludin at the tight junction (Fig. 1E, bottom). To confirm that the GFP moiety did not influence subcellular targeting, visualization of HA-tagged paracellin-1 (FL and △70) using an HA antibody produced similar results (images not shown). Intriguingly, genetic analysis of FHHNC patients has identified a point mutation M71R linked to FHHNC (Fig. 5A) (Simon et al., 1999), thus highlighting the functional significance of △70-paracellin-1. As FL-paracellin-1 fails to translocate to tight junctions, it is possible that in humans the native cellular environment of the thick ascending limb of the nephron contains regulatory factors to allow bypassing the first methionine (M1) in paracellin-1 and ensure appropriate translation from the second methionine (M71). Definitive evidence for this speculation requires an investigation of the size of translational product of paracellin-1 in human kidney. In the following studies, we will focus upon △70-paracellin-1 and refer to it simply as paracellin-1.

Paracellin-1 function

To determine the function of paracellin-1, we have expressed paracellin-1 in well-established epithelial cell models (e.g. MDCK-II and LLC-PK1 cells) (Fig. 2A). Neither of these cell lines expressed endogenous paracellin-1 (control cells were infected with an empty vector). Staining with the paracellin-1 antibody showed its localization in the tight junction (Fig. 2B showing MDCK-II cells as a representative), further corroborating our findings described above. As we aimed to have cells expressing paracellin-1 during a prolonged period so that they could become fully polarized and form tight junction (normally >10 days), we utilized a retroviral expression system to generate the VSV-G-pseudotyped retrovirus (titer used at 1×10^6 cfu/ml) capable of infecting a wide range of cell types and integrating into the host genome. Over 95% of infected cells expressed paracellin-1 in a homogenous manner (see supplementary material Fig. S1), without further clonal selection or antibiotic selection. This homogenous expression of paracellin-1 persisted when cells became polarized (after being seeded onto Transwell plates). On day 12 post polarization, cell monolayers were subjected to electrophysiological measurements and immunostained to visualize paracellin-1 localization (Fig. S2). We have assayed the expression levels of other endogenous claudins (claudin 1-4 in MDCK-II cells; claudin-1, -3 and -4 in LLC-PK1 cells with no claudin-2 expression) with or without the ectopic expression of paracellin-1 and found no differences in the protein levels (data not shown).

In LLC-PK1 cells, we found that paracellin-1 profoundly increased the permeability of Na^+ (P_{Na}) without significant effects on Cl^- (P_{Cl}) (Fig. 3A). When we challenged the LLC-PK1 monolayer (12 days post polarization) with an apical-to-basal chemical gradient (145 mM NaCl at the apical side to 80 mM at the basal side), we found that a –8.20±0.12 mV diffusion potential had developed across the monolayer (with the apical side as zero reference), indicating that the junctional pores of LLC-PK1 cells were more permeable to anions than cations. Paracellin-1 significantly increased the diffusion potential to +1.40±0.06 mV (P<0.001, n=3; Fig. 3B). The experiment was also performed with a basal-to-apical chemical gradient (with the basal side as zero reference) and we found

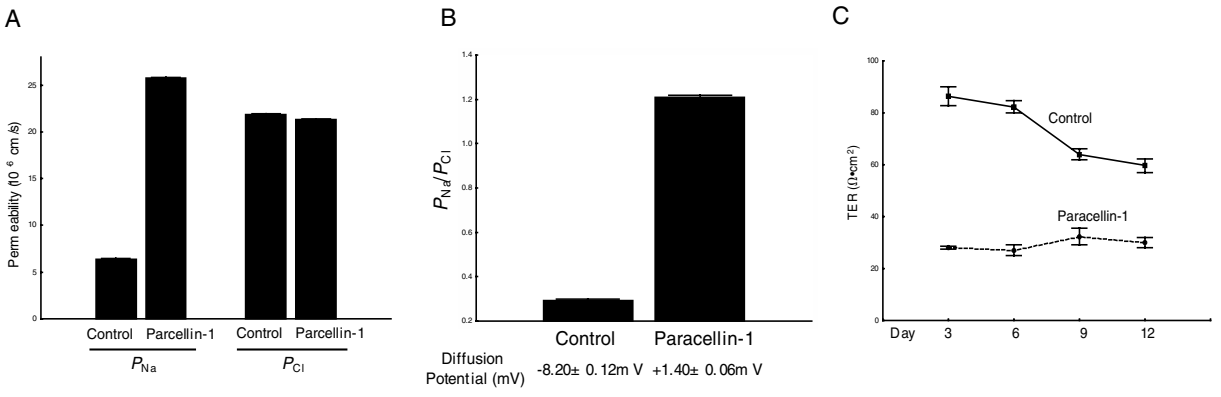

D

	P_{Li} (10^{-6}cm/s)	P_{Na} (10^{-6}cm/s)	P_{K} (10^{-6}cm/s)	P_{Rb} (10^{-6}cm/s)	P_{Cs} (10^{-6}cm/s)	P_{Mg} (10^{-6}cm/s)
Control	9.101±0.107	6.381±0.107	5.753±0.099	5.370±0.205	5.175±0.104	6.564±0.023
Paracellin-1	28.810±0.180	25.750±0.092	29.630±0.270	26.577±0.057	25.083±0.055	10.740±0.059

Fig. 3. Function of paracellin-1. (A) Effects of paracellin-1 on the permeability of Na^+ and Cl^- in LLC-PK1 cells. (B) Ratio of P_{Na} to P_{Cl} and diffusion potential (bottom) across a LLC-PK1 cell monolayer. (C) TER across an LLC-PK1 cell monolayer over a period of 12 days in cells expressing paracellin-1 and control cells. (D) Summary of the effects of paracellin-1 upon permeability of various cations in LLC-PK1 cells.

the direction of gradient had no effects on our measurements of diffusion potential. The Goldman-Hodgkin-Katz equation calculated the ratio of permeability of Na^+ over Cl^- at 0.29±0.01 in control cells compared to 1.21±0.01 in cells expressing paracellin-1 (P<0.001) (Fig. 3B). This suggested that paracellin-1 altered the ion selectivity of tight junctions to favor cation permeation between LLC-PK1 cells. Measuring the TER (in 145 mM NaCl) and applying the Ohm's law allowed us to determine the permeability of Na^+ and Cl^- in LLC-PK1 cells respectively (see Fig. 3A; Table 1). As shown in Fig. 3C, TER was significantly lowered by paracellin-1 in LLC-PK1 cells over a period of 12 days, owing to its stimulation of Na^+ flux. Addition of 1 mM ouabain (Na^+/K^+-ATPase inhibitor) to the basolateral side had no effects on P_{Na} or P_{Cl} in both control and paracellin-1-expressing cells, indicating a paracellular pathway for ion flux. This experiment was repeated and confirmed independently twice with three separate monolayers. A similar effect was also seen with other monovalent alkali metal cations (including Li^+, K^+, Rb^+ and Cs^+; see Fig. 3D). An effect of paracellin-1 on P_{Mg} was found in LLC-PK1 cells which showed a small but significant increase in P_{Mg} (Fig. 3D).

Expression of paracellin-1 mutants

To elucidate the mechanism of function of paracellin-1, we have generated a run of single or multiple point mutations in paracellin-1. We focused these mutations on the first extracellular loop and on known human mutations in the paracellin-1 gene. The profile of expression and localization of mutants are summarized in Table 1, Fig. 4A-D and supplementary material Fig. S2. To normalize the expression among various mutants and with the wild type, we infected cells with a fixed titer of virus at 1×10^6 cfu/ml and quantified the transcription of the transgene by RT-PCR. Although we did not find variation among mutants at the level of transcription, a number of mutant proteins (L167P, G198D, R216T, G233D) were not expressed by cells (not detectable using western blotting or immunofluorescence staining), suggesting that that these mutations had rendered proteins unstable and triggered a degradation signal. A number of mutant proteins (D97S, R149L, R149T, S235P and G239R) were sequestered in the ER showing a reticular cytoplasmic and perinuclear distribution, or Golgi apparatus showing tubular structures close to the periphery of the nucleus (Fig. 4E). This suggests that the points of mutation played roles in protein folding, ER quality control or protein trafficking. These mutants were also difficult to express (a weak band upon immunoblotting) and were maintained at a low level by cells. The rest of the mutant proteins were expressed at a comparable level to the wild type, and all localized to the tight junction (see Fig. S2 in supplementary material).

Structural requirements of paracellin-1 function

We generated a series of point mutations on amino acids in paracellin-1 to identify amino acid(s) crucial for its function. The first extracellular loop of paracellin-1 is enriched with negatively charged amino acids (underlined in Fig. 4A; in yellow in Fig. 5A; also see alignment of claudins in supplementary material Fig. S3). We have systematically removed the charge from each of the ten negatively charged amino acids by mutagenesis (mutated to serine or threonine) to study the effects of charge upon the function of paracellin-1 in LLC-PK1 cells. A summary of the mutants and their levels of expression is shown in Fig. 4B. A summary of the physiological changes resulting from the mutations is shown in Table 1. All single mutations in the first extracellular loop

Table 1. Mutations affecting the function of paracellin-1

Construct	Position of mutation	Expression	Localisation	TER ($\Omega \cdot cm^2$)	P_{Na}/P_{Cl}	P_{Na} (10^{-6} cm/second)	P_{Cl} (10^{-6} cm/second)	Function
vector	–	–	–	65.0	0.292±0.006	6.381±0.107	21.857±0.107	–
WT	–	+	TJ	39.0	1.208±0.009	25.750±0.092	21.310±0.092	+
L167P	2nd TMD	–	–	53.0	0.262±0.002	7.183±0.038	27.450±0.040	–
G198D	3rd TMD	–	–	59.3	0.272±0.005	6.656±0.090	24.453±0.091	–
R216T	2nd ECL	–	–	46.3	0.336±0.007	10.023±0.159	29.873±0.156	–
G233D	2nd ECL	–	–	50.3	0.279±0.005	8.015±0.106	28.690±0.106	–
D97S	1st ECL	weak	ER	42.0	0.262±0.019	9.065±0.530	34.633±0.530	–
R149L	1st ECL	weak	ER	54.0	0.300±0.009	7.830±0.186	26.157±0.187	–
R149T	1st ECL	weak	ER	52.0	0.336±0.010	8.868±0.140	26.430±0.139	–
S235P	2nd ECL	weak	ER	54.3	0.273±0.017	7.273±0.366	26.717±0.364	–
G239R	4th TMD	+	Golgi	57.0	0.382±0.006	8.906±0.094	23.297±0.094	–
D104S	1st ECL	+	TJ	36.0	0.607±0.010	19.260±0.206	31.723±0.208	partial –
D105S	1st ECL	+	TJ	36.7	0.843±0.015	22.683±0.223	26.917±0.223	partial –
E119T	1st ECL	+	TJ	36.3	0.816±0.006	22.917±0.101	28.070±0.098	partial –
D126S	1st ECL	+	TJ	43.0	0.770±0.004	18.563±0.047	24.120±0.050	partial –
E140T	1st ECL	+	TJ	44.0	0.692±0.011	17.063±0.165	24.650±0.162	partial –
Mut^{3ST}	1st ECL	+	TJ	60.3	0.706±0.029	12.650±0.303	17.940±0.303	partial –
Mut^{6ST}	1st ECL	+	TJ	69.7	0.960±0.007	12.843±0.049	13.373±0.049	partial –
L145P	1st ECL	+	TJ	41.7	0.470±0.009	13.977±0.174	29.723±0.174	partial –
L151F	1st ECL	+	TJ	43.7	0.696±0.006	17.107±0.093	24.603±0.093	partial –
G191R	3rd TMD	+	TJ	47.0	0.777±0.016	17.070±0.192	21.980±0.192	partial –
A209T	2nd ECL	+	TJ	34.7	0.643±0.008	20.513±0.156	31.927±0.156	partial –
E108T	1st ECL	+	TJ	40.7	1.051±0.019	22.937±0.203	21.830±0.200	+
D132S	1st ECL	+	TJ	36.0	1.320±0.052	28.983±0.497	22.003±0.500	+
E133T	1st ECL	+	TJ	40.3	1.032±0.009	23.307±0.103	22.583±0.103	+
D135S	1st ECL	+	TJ	40.0	1.197±0.005	25.003±0.053	20.880±0.050	+
F232C	2nd ECL	+	TJ	29.0	0.996±0.004	31.570±0.070	31.713±0.073	+
K112S	1st ECL	+	TJ	37.3	1.254±0.029	27.587±0.277	22.020±0.280	+
R114T	1st ECL	+	TJ	34.3	0.944±0.018	26.203±0.264	27.777±0.264	+
R129T	1st ECL	+	TJ	34.0	1.289±0.032	30.387±0.337	23.593±0.337	+
K144S	1st ECL	+	TJ	39.7	1.259±0.020	25.570±0.179	20.313±0.176	+

ECL, extracellular loop; ER, endoplasmic reticulum; Golgi, Golgi apparatus; TJ, tight junction; TMD, transmembrane domain; +, showing the function of paracellin-1; –, abolishing the function of paracellin-1.

expressed at equivalent levels and localized to the tight junction, except D97S that showed weak expression and only a cytoplasmic localization. As shown above in LLC-PK1 cells, the wild-type (WT) paracellin-1 increased the ratio between P_{Na} and P_{Cl} by upregulating Na^+ passage. As expected, D97S was unable to increase either the diffusion potential of NaCl (Fig. 5B red circle) or the ratio of P_{Na} to P_{Cl} (D97S, 0.26±0.02 vs WT, 1.21±0.01; $P<0.001$; Fig. 5C), consistent with the fact that it was not localized to the tight junction (Fig. 4E). Mutations (D104S, D105S, E119T, D126S and E140T) caused a significant (but not complete) loss of function in paracellin-1 (diffusion potential in Fig. 5B blue circle; P_{Na}/P_{Cl} D104S, 0.61±0.01; D105S, 0.84±0.02; E119T, 0.82±0.01; D126S, 0.77±0.004; E140T, 0.69±0.01; $P<0.01$ vs WT values; Fig. 5C). The remaining mutations, E108T, D132S, E133T and D135S did not significantly alter paracellin-1 function compared to WT levels.

To determine whether the effects of charge were additive, we mutated the negatively charged amino acids in groups. We generated four mutants to combine the point mutations described above (Mut^{3ST}, Mut^{4ST}, Mut^{6ST} and Mut^{10ST}; Fig. 4B). The Mut^{4ST} and the Mut^{10ST} contained the non-functional D97S mutation and both these were undetectable. Only two mutants (Mut^{3ST} and Mut^{6ST}) were expressed successfully and localized at the tight junction. Both types of mutation result in the lowest Na^+ permeability of all constructs that localize to the tight junction (Table 1). This suggested that the effects of charge were additive and not independent. As a control, mutations on the positively charged amino acids (K or R in Fig. 4A, marked in bold and italic) in the first extracellular loop (to remove their charges: K112S, R114T, R129T and K144S) had no effects on the function of paracellin-1 (except that R149T was confined to the ER and showed a complete loss of function; see Table 1 and Fig. 4C).

Genetic analysis has linked 12 distinct missense mutations in paracellin-1 to FHHNC (Fig. 5A, red dots) (Simon et al., 1999; Weber et al., 2001a). These mutations provided us with a natural source of identifying loss-of-function mutations in paracellin-1. Most of the mutations were found in the extracellular loops of paracellin-1 (L145P, R149L and L151F in the first extracellular loop; A209T, R216T, F232C, G233D and S235P in the second extracellular loop). The rest were in the transmembrane domains (L167P, G191R, G198D and G239R). We found that all of these mutations (except F232C) caused paracellin-1 to lose its function (studied in LLC-PK1 cells). In particular, mutations (R149L, L167P, G198D, R216T and G233D) led to a complete loss of function (diffusion potential in Fig. 5D red circle; P_{Na}/P_{Cl} R149L, 0.30±0.01; L167P, 0.26±0.002; G198D, 0.27±0.01; R216T, 0.34±0.01; G233D, 0.28±0.01; S235P, 0.27±0.02; G239R, 0.38±0.01. $P<0.001$ vs WT levels; Fig. 5E). We have also found that the mutants R149L, S235P and G239R were confined to the ER or Golgi apparatus (Fig. 4E) whereas L167P, G198D, R216T and G233D were not stably expressed by cells (Fig. 4D). The remaining mutants (L145P, L151F, G191R and A209T) were expressed well and found in the tight junction. They showed a

Journal of Cell Science

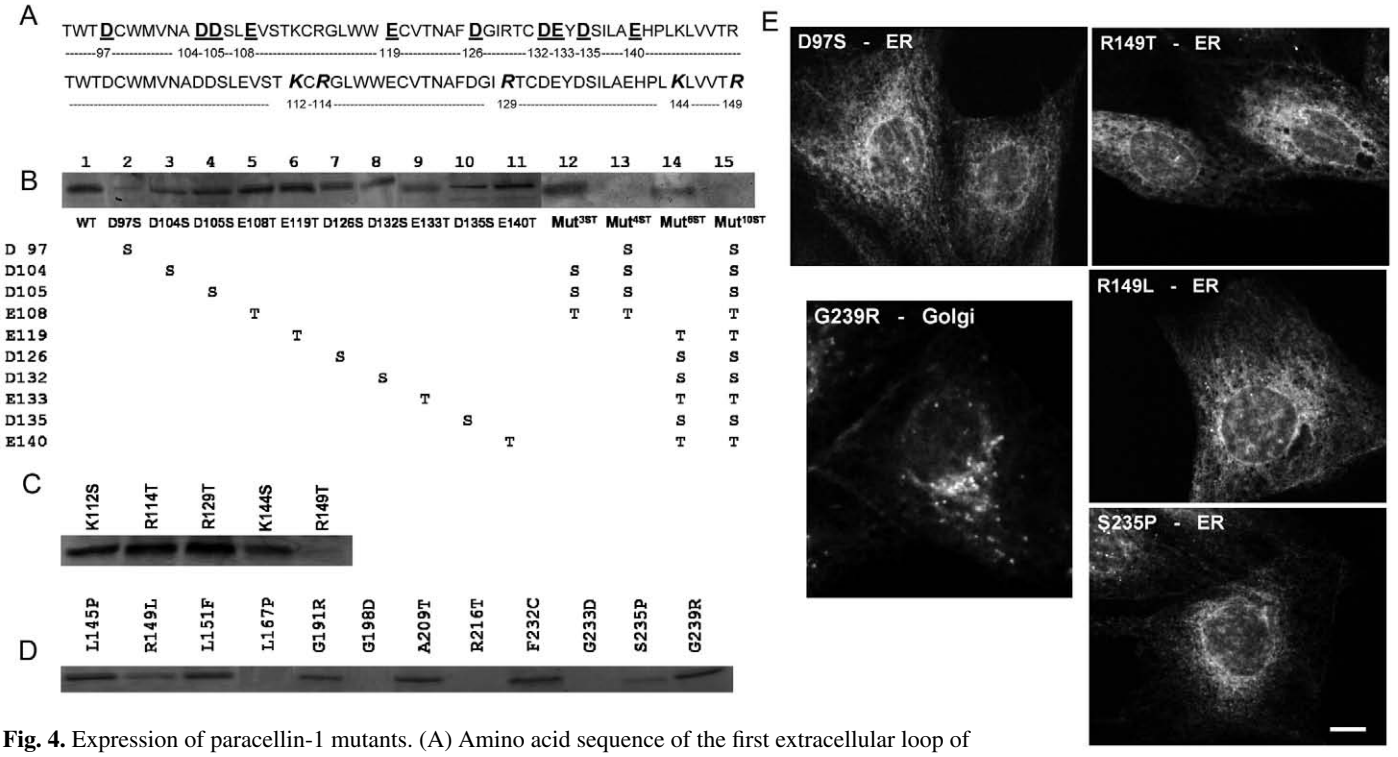

Fig. 4. Expression of paracellin-1 mutants. (A) Amino acid sequence of the first extracellular loop of paracellin-1. Negatively charged amino acids are labeled in bold and underlined; positively charged amino acids are in bold italics. (B-D) Protein immunoblots of expression of paracellin-1 mutants. (B) Mutations to replace the negatively charged amino acids (D or E) with S or T. Names of mutants are shown underneath the blot, followed by the positions of mutations. (C) Mutations to replace the positively charged amino acids (K or R) with S or T. (D) Mutations found in human patients with FHHNC. (E) Gallery of epifluorescence images showing mis-targeted localization of paracellin-1 mutants in LLC-PK1 cells. D97S, R149T, R149L and S235P in the ER; G239R in the Golgi apparatus. The ER shows a reticular cytoplasmic and perinuclear distribution and the Golgi apparatus tubular structures close to the periphery of the nucleus. Bar, 10 μm.

significant (but not complete) loss of function compared to WT paracellin-1 (diffusion potential in Fig. 5D blue circle; P_{Na}/P_{Cl} L145P, 0.47±0.01; L151F, 0.70±0.01; G191R, 0.78±0.01; and A209T, 0.64±0.01; $P<0.01$ vs WT).

One more replicate infection was performed for all the mutants to independently confirm the data above (each with three separate monolayers). The full set of data (expression, localization, TER, P_{Na}, P_{Cl} and P_{Na}/P_{Cl}) on all mutants described above is summarized in Table 1.

Discussion

Our data suggest that paracellin-1 functions to modulate paracellular conductance and not transcellular transport. LLC-PK1 cells are well-established cell models in investigating paracellular conductance. In these cells, paracellular conductance greatly exceeds transcellular conductance owing to their low TER (<100 $\Omega\cdot cm^2$). The current-voltage relationship of the TER is linear and symmetrical in these monolayers. Transmembrane carriers such as ion channels and transporters are expected to have a limited capacity to conduct current and thus to have a nonlinear *I-V* curve. Blocking the transcellular pathway by inhibiting the basolateral Na^+/K^+-ATPase (1 mM ouabain) had no effect on transepithelial conductance. We have identified key amino acids in the extracellular loops of paracellin-1 that are critical for its function. The extracellular loops of claudins are believed to mediate homophilic or heterophilic interactions between claudins (see Turksen and Troy, 2004). Mutations of these amino acids resulted in a loss of function without affecting protein expression or trafficking. Taken together, it is unlikely that the function of paracellin-1 involves signaling cascades and/or other transmembrane carriers to switch on a transcellular pathway.

Micropuncture studies have shown that ~50-60% of filtered Mg^{2+} is reabsorbed in the loop of Henle, primarily through the thick ascending limb (TAL) (Quamme and Dirks, 1980). A number of elegant in vitro studies using perfused TAL tubules have examined the relationship between the flux of Mg^{2+} and the transepithelial voltage (V_t) (Di Stefano et al., 1993; Hebert and Andreoli, 1986; Mandon et al., 1993; Shareghi and Agus, 1982). The flux-voltage relationship with identical Mg^{2+} concentration on both sides of the perfused tubule indicates that at zero voltage the net transport of Mg^{2+} is zero. With a lumen-positive V_t, Mg^{2+} is reabsorbed, whereas with a lumen-negative V_t, Mg^{2+} is secreted. The dependence of Mg^{2+} reabsorption on transepithelial voltage suggests a passive process via the paracellular pathway. When TAL is perfused with isotonic NaCl solutions, the lumen voltage is positive at 3-10 mV owing to apical membrane K^+ secretion (Greger and Schlatter, 1983). In the process of urine dilution and concentration, the reabsorption of NaCl is separated from that of H_2O in TAL (as TAL is highly impermeable to H_2O), resulting in diluted tubule fluid in the lumen and a high

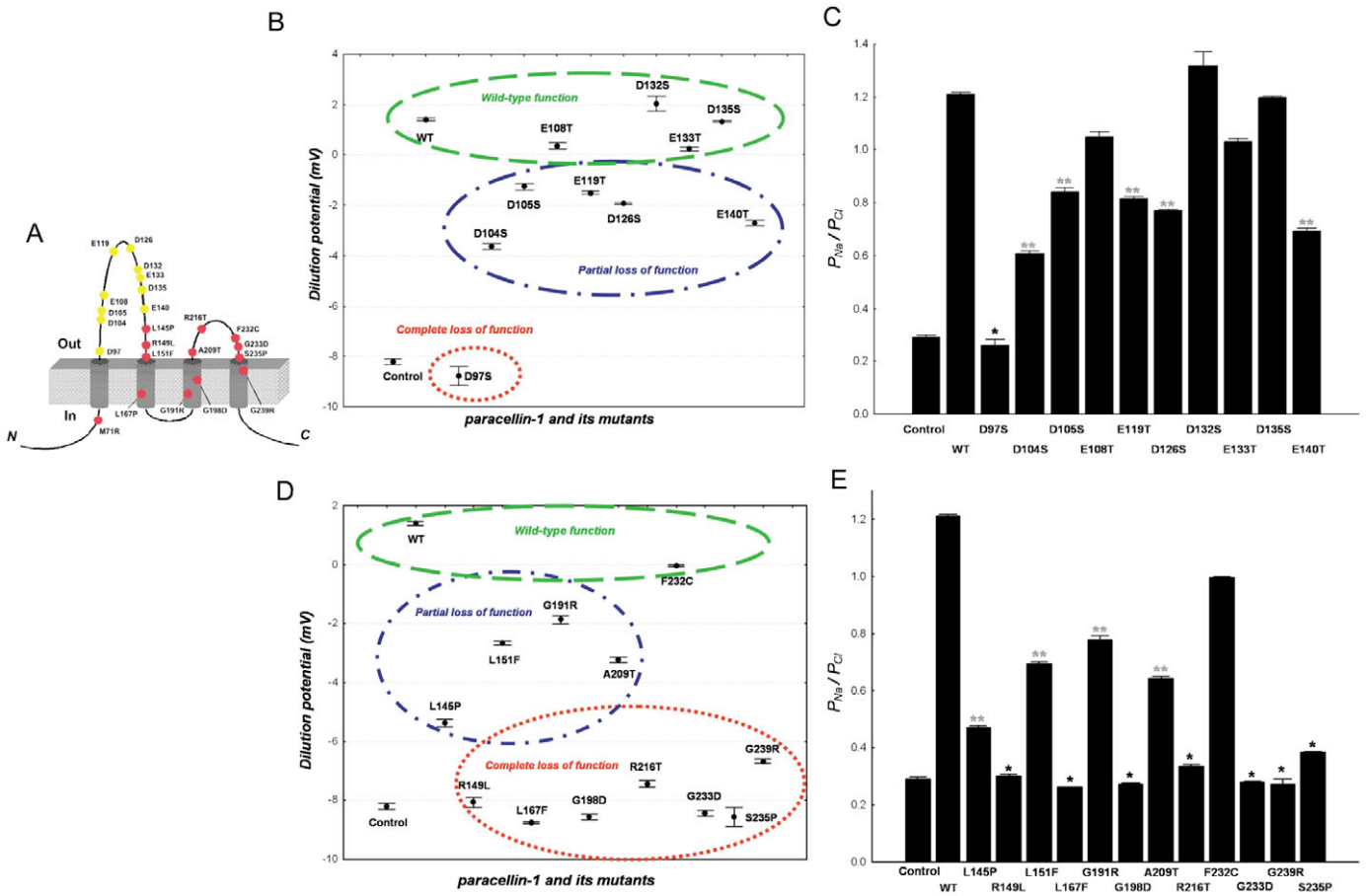

Fig. 5. Structural requirements of paracellin-1 function. (A) Mutations in paracellin-1. Yellow dots, negatively charged amino acids; red dots, mutations found in patients having FHHNC. (B) and (D) Effects of paracellin-1 and its mutants upon dilution potential across LLC-PK1 cell monolayers. (C and E) Effects of paracellin-1 and its mutants upon the ratio of P_{Na} to P_{Cl} (correlated to the values of diffusion potential in B and D respectively). *P<0.001 and **P<0.01 compared to ratio in the WT.

concentration of NaCl in the peritubular space. A transcellular NaCl concentration gradient (from peritubular space to lumen) develops and becomes pronounced (up to 120 mM in the cortical TAL and 60 mM in the medullary TAL). Because the paracellular pathway in TAL is cation selective (with a P_{Na}/P_{Cl} value between 2 and 4) (Greger, 1981), the transepithelial voltage increases to as much as 30 mV, with the lumen positive (Rocha and Kokko, 1973; Greger, 1981), as a result of the diffusion potential generated by the back-flow of Na^+ from peritubular space to tubule lumen down its concentration gradient via the paracellular pathway. This large voltage drives the bulk of reabsorption of Mg^{2+}. We have found that paracellin-1 modulates the ion selectivity of the tight junction to increase the ratio of P_{Na}/P_{Cl} in LLC-PK1 cells. It is not unreasonable to suspect that paracellin-1 plays a similar role in modulating ion selectivity in TAL cells and thus controls the level of transepithelial voltage (the primary driving force for Mg^{2+} reabsorption). A loss of function in paracellin-1 in TAL could lead to a decrease in P_{Na}/P_{Cl}, therefore losing the lumen-positive voltage or even reversing its sign and eventually the renal wasting of Mg^{2+}. The handling of Ca^{2+} in TAL follows the same pathway as that of Mg^{2+}. This hypothesis is being actively tested by using siRNA to knockdown paracellin-1 function in TAL both ex vivo and in vivo.

We found that in LLC-PK1 cells (showing anion selectivity) paracellin-1 affected the permeation of cations (P_{Na}) and increased the ratio of P_{Na} to P_{Cl}. However, in MDCK-II cells (showing cation selectivity), we found no significant effects of paracellin-1 on P_{Na}, P_{Cl} or P_{Mg}. Our results are consistent with a model in which exogenous claudins add new charge-selective pores leading to a physiological phenotype that combines contributions of both endogenous and exogenous claudins in the cell. These data are consistent with other studies. For example, claudin-2 has little effect on TER in MDCK II cells, whereas in LLC-PK cells it causes a decrease in TER (Van Itallie et al., 2003) similar to that described in MDCK-I cells (Furuse et al., 2001; Amasheh et al., 2002). Expression of claudin-11 or -15, which causes a significant increase in TER in MDCK-II cells, instead decreases TER in LLC-PK1 cells (Van Itallie et al., 2003). Although not much biochemical data are yet available, the variations in physiology measured following expression of claudins in different epithelial cell lines suggests that they take part in both homophilic and heterophilic interactions.

Claudins have long been established as constituents of the

Journal of Cell Science

Journal of Cell Science

tight junction (TJ) strands (a linear proteinaceous polymer spanning plasma membranes) (Furuse et al., 1998a; Furuse et al., 1998b). When exogenously expressed in L fibroblasts, claudins polymerize into paired strands via both homophilic and heterophilic adhesions (Furuse et al., 1999). Different modes of assembly of claudins apparently increase the diversity of the structure of the TJ strands, providing a molecular basis for the heterogeneity of TJ functions. The extracellular loops of claudins, whose sequences are distinct in different claudins, contribute to the formation not only of TJ strands but also of ion-selective channels or barriers. Our studies have supported this hypothesis in that the majority of loss-of-function mutations of paracellin-1 were found in the extracellular loops. In particular, our findings have highlighted the importance of the negatively charged amino acids (D104S, D105S, E119T, D126S and E140T) in the first extracellular loop. However, none of these mutations (single or in combination) completely abolished the function of paracellin-1, suggestive of involvement of other functional components. Although we have found a number of mutations (D97S, R149L, L167P, G198D, R216T, G233D, S235P and G239R) resulting in a complete loss of function, these mutations either caused the protein to become unstable or to fail to correctly traffic to the plasma membrane. Paracellin-1 mutants that successfully translocated to the TJ, however, altered ion permeability to varying degrees, indicating possible interactions with endogenous molecules. It is likely that paracellin-1 takes part in two types of protein-protein interactions. First, the homophilic interactions between paracellin-1 lead to the formation of a cation-conducting pore in LLC-PK1 cells. The charged amino acids in the first extracellular loop may directly affect cation permeation. The mutations (L145P, L151F, G191R and A209T) found in the transmembrane domains and the extracellular loops may distort the structural conformation of the pore. Second, the heterophilic interactions between paracellin-1 and other claudins may modulate endogenous ion-conducting properties. It is currently not known which claudin(s) paracellin-1 interacts with, although the principle of specific claudin-claudin interactions has been demonstrated (Furuse et al., 1999).

We thank Joan Brugge for providing the retroviral expression system and Vivian Tang for several epithelial cell lines. We also thank Friso Postma for his thoughtful suggestions on this work. We are grateful to the Nikon Imaging Centre (Harvard Medical School) for their excellent assistance on confocal microscopy. Supported by GM18974 and GM37751 from the NIH.

References

Amasheh, S., Meiri, N., Gitter, A. H., Schoneberg, T., Mankertz, J., Schulzke, J. D. and Fromm, M. (2002). Claudin-2 expression induces cation-selective channels in tight junctions of epithelial cells. *J. Cell. Sci.* **115**, 4969-4976.

Anderson, J. M., Van Itallie, C. M. and Fanning, A. S. (2004). Setting up a selective barrier at the apical junction complex. *Cur. Opin. Cell Biol.* **16**, 140-145.

Ben-Yosef, T., Belyantseva, I. A., Saunders, T. L., Hughes, E. D., Kawamoto, K., Van Itallie, C. M., Beyer, L. A., Halsey, K., Gardner, D. J., Wilcox, E. R. et al. (2003). Claudin 14 knockout mice, a model for autosomal recessive deafness DFNB29, are deaf due to cochlear hair cell degeneration. *Hum. Mol. Genet.* **12**, 2049-2061.

Blanchard, A., Jeunemaitre, X., Coudol, P., Dechaux, M., Froissart, M., May, A., Demontis, R., Fournier, A., Paillard, M. and Houillier, P. (2001). Paracellin-1 is critical for magnesium and calcium reabsorption in the human thick ascending limb of Henle. *Kidney Intl.* **59**, 2206-2215.

Claude, P. (1978). Morphological factors influencing transepithelial permeability: a model for the resistance of the zonula occludens. *J. Membr. Biol.* **39**, 219-232.

Claude, P. and Goodenough, D. A. (1973). Fracture faces of zonulae occludentes from 'tight' and 'leaky' epithelia. *J. Cell Biol.* **58**, 390-400.

Colegio, O. R., Van Itallie, C. M., McCrea, H. J., Rahner, C. and Anderson, J. M. (2002). Claudins create charge-selective channels in the paracellular pathway between epithelial cells. *Am. J. Physiol. Cell Physiol.* **283**, C142-C147.

De Rouffignac, C. and Quamme, G. (1994). Renal magnesium handling and its hormonal control. *Physiol. Rev.* **74**, 305-322.

Di Stefano, A., Roinel, N., De Rouffignac, C. and Wittner, M. (1993). Transepithelial Ca^{2+} and Mg^{2+} transport in the cortical thick ascending limb of Henle's loop of the mouse is a voltage-dependent process. *Renal Physiol. Biochem.* **16**, 157-166.

Fromter, E. and Diamond, J. (1972). Route of passive ion permeation in epithelia. *Nat. New Biol.* **235**, 9-13.

Furuse, M., Hirase, T., Itoh, M., Nagafuchi, A., Yonemura, S. and Tsukita, S. (1993). Occludin: a novel integral membrane protein localizing at tight junctions. *J. Cell Biol.* **123**, 1777-1788.

Furuse, M., Fujita, K., Hiiragi, T., Fujimoto, K. and Tsukita, S. (1998a). Claudin-1 and -2: novel integral membrane proteins localizing at tight junctions with no sequence similarity to occludin. *J. Cell Biol.* **141**, 1539-1550.

Furuse, M., Sasaki, H., Fujimoto, K. and Tsukita, S. (1998b). A single gene product, claudin-1 or -2, reconstitutes tight junction strands and recruits occludin in fibroblasts. *J. Cell Biol.* **143**, 391-401.

Furuse, M., Sasaki, H. and Tsukita, S. (1999). Manner of interaction of heterogeneous claudin species within and between tight junction strands. *J. Cell Biol.* **147**, 891-903.

Furuse, M., Furuse, K., Sasaki, H. and Tsukita, S. (2001). Conversion of zonulae occludentes from tight to leaky strand type by introducing claudin 2 into Madin-Darby canine kidney I cells. *J. Cell Biol.* **153**, 263-272.

Greger, R. (1981). Cation selectivity of the isolated perfused cortical thick ascending limb of Henle's loop of rabbit kidney. *Pflugers Arch.* **390**, 30.

Greger, R. (1985). Ion transport mechanisms in thick ascending limb of Henle's loop of mammalian nephron. *Physiol. Rev.* **65**, 760-797.

Greger, R. and Schlatter, E. (1983). Properties of the lumen membrane of the cortical thick ascending limb of Henle's loop of rabbit kidney. *Pflugers Arch.* **396**, 315.

Hebert, J. C. and Andreoli, T. E. (1986). Ionic conductance pathways in the mouse medullary thick ascending limb of Henle. *J. Gen. Physiol.* **87**, 567-590.

Mandon, B., Siga, E., Roinel, N. and De Rouffignac, C. (1993). Ca^{2+}, Mg^{2+} and K^{+} transport in the cortical and medullary thick ascending limb of the rat nephron: influence of transepithelial voltage. *Pflugers Arch.* **424**, 558-560.

Morita, K., Furuse, M., Fujimoto, K. and Tsukita, S. (1999). Claudin multigene family encoding four-transmembrane domain protein components of tight junction strands. *Proc. Natl. Acad. Sci. USA* **96**, 511-516.

Muller, D., Kausalya, P. J., Claverie-Martin, F., Meij, I. C., Eggert, P., Garcia-Nieto, V. and Hunziker, W. (2003). A novel claudin 16 mutation associated with childhood hypercalciuria abolishes binding to ZO-1 and results in lysosomal mistargeting. *Am. J. Hum. Genet.* **73**, 1293-1301.

Quamme, G. A. and Dirks, J. H. (1980). Magnesium transport in the nephron. *Am. J. Physiol.* **239**, F393-F401.

Rocha, A. S. and Kokko, J. P. (1973). Sodium chloride and water transport in the medullary thick ascending limb of Henle: Evidence for active chloride transport. *J. Clin. Invest.* **52**, 612.

Schneeberger, E. E. and Lynch, R. D. (2004). The tight junction: a multifunctional complex. *Am. J. Physiol. Cell Physiol.* **286**, C1213-C1228.

Shareghi, G. R. and Agus, Z. S. (1982). Magnesium transport in the cortical thick ascending limb of Henle's loop of the rabbit. *J. Clin. Invest.* **69**, 759-769.

Simon, D. B., Lu, Y., Choate, K. A., Velazquez, H., Al-Sabban, E., Praga, M., Casari, G., Bettinelli, A., Colussi, G., Rodriguez-Soriano, J. et al. (1999). Paracellin-1, a renal tight junction protein required for paracellular Mg^{2+} resorption. *Science* **285**, 103-106.

Tang, V. W. and Goodenough, G. A. (2003). Paracellular ion channel at the tight junction. *Biophys. J.* **84**, 1660-1673.

Tsukita, S., Furuse, M. and Itoh, M. (2001). Multifunctional strands in tight junctions. *Nat. Rev. Mol. Cell. Biol.* **2**, 285-293.

Turksen, K. and Troy, T. C. (2004). Barriers built on claudins. *J. Cell. Sci.* **117**, 2435-2477.

Van Itallie, C., Rahner, C. and Anderson, J. M. (2001). Regulated expression of claudin-4 decreases paracellular conductance through a selective decrease in sodium permeability. *J. Clin. Invest.* **107**, 1319-1327.

Van Itallie, C., Fanning, A. S. and Anderson, J. M. (2003). Reversal of charge selectivity in cation or anion-selective epithelial lines by expression of different claudins. *Am. J. Physiol. Renal Physiol.* **285**, F1078-F1084.

Weber, S., Schneider, L., Peters, M., Misselwitz, J., Ronnefarth, G., Boswald, M., Bonzel, K. E., Seeman, T., Sulakova, T., Kuwertz-Broking, E. et al. (2001a). Novel paracellin-1 mutations in 25 families with familial hypomagnesemia with hypercalciuria and nephrocalcinosis. *J. Am. Soc. Nephrol.* **12**, 1872-1881.

Weber, S., Schlingmann, K. P., Peters, M., Nejsum, L. N., Nielsen, S., Engel, H., Grzeschik, K. H., Seyberth, H. W., Grone, H. J., Nusing, R. et al. (2001b). Primary gene structure and expression studies of rodent paracellin-1. *J. Am. Soc. Nephrol.* **12**, 2664-2672.

Wen, H., Watry, D. D., Marcondes, M. C. G. and Fox, S. H. (2004). Selective decrease in paracellular conductance of tight junctions: role of the first extracellular domain of claudin-5. *Mol. Cell. Biol.* **24**, 8408-8417.

Yu, A. S. L., Enck, A. H., Lencer, W. I. and Schneeberger, E. E. (2003). Claudin-8 expression in Madin-Darby canine kidney cells augments the paracellular barrier to cation permeation. *J. Biol. Chem.* **278**, 17350-17359.

Journal of Cell Science